ACS APPLIED MATERIALS & INTERFACES

Research Article

www.acsami.org

Nonequilibrium Self-Assembly of π-Conjugated Oligopeptides in Solution

Bo Li,[†] Songsong Li,[‡] Yuecheng Zhou,[‡] Herdeline Ann M. Ardoña,[§] Lawrence R. Valverde,[‡] William L. Wilson,[‡,∥,⊥] John D. Tovar,[§,#] and Charles M. Schroeder*[,†,‡]

[†]Department of Chemical and Biomolecular Engineering, University of Illinois at Urbana−Champaign, Urbana, Illinois 61801, United States

[‡]Department of Materials Science and Engineering, University of Illinois at Urbana−Champaign, Urbana, Illinois 61820, United States

[§]Department of Chemistry, Johns Hopkins University, Baltimore, Maryland 21218, United States

[∥]Frederick Seitz Materials Research Laboratory, University of Illinois at Urbana−Champaign, Urbana, Illinois 61801, United States

[⊥]Center for Nanoscale Systems, Faculty of Arts and Sciences, Harvard University, Cambridge, Massachusetts 02138, United States

[#]Department of Materials Science and Engineering, Johns Hopkins University, Baltimore, Maryland 21218, United States

Supporting Information

ABSTRACT: Supramolecular assembly is a powerful method that can be used to generate materials with well-defined structures across multiple length scales. Supramolecular assemblies consisting of biopolymer−synthetic polymer subunits are specifically known to exhibit exceptional structural and functional diversity as well as programmable control of noncovalent interactions through hydrogen bonding in biopolymer subunits. Despite recent progress, there is a need to control and quantitatively understand assembly under nonequilibrium conditions. In this work, we study the nonequilibrium self-assembly of π-conjugated synthetic oligopeptides using a combination of experiments and analytical modeling. By isolating an aqueous peptide solution droplet within an immiscible organic layer, the rate of peptide assembly in the aqueous solution can be controlled by tuning the transport rate of acid that is used to trigger assembly. Using this approach, peptides are guided to assemble under reaction-dominated and diffusion-dominated conditions, with results showing a transition from a diffusion-limited reaction front to spatially homogeneous assembly as the transport rate of acid decreases. Interestingly, our results show that the morphology of self-assembled peptide fibers is controlled by the assembly kinetics such that increasingly homogeneous structures of self-assembled synthetic oligopeptides were generally obtained using slower rates of assembly. We further developed an analytical reaction−diffusion model to describe oligopeptide assembly, and experimental results are compared to the reaction−diffusion model across a range of parameters. Overall, this work highlights the importance of molecular self-assembly under nonequilibrium conditions, specifically showing that oligopeptide assembly is governed by a delicate balance between reaction kinetics and transport processes.

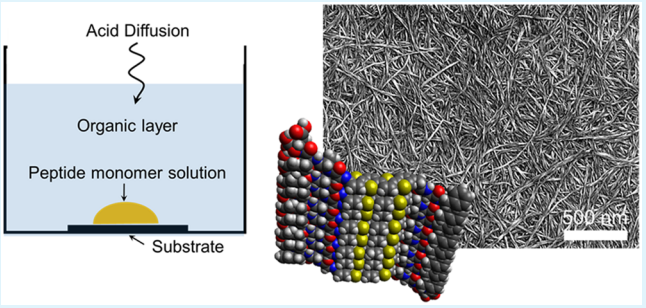

KEYWORDS: *supramolecular assembly, biohybrid materials, optoelectronic materials, nonequilibrium assembly, reaction-controlled, diffusion-controlled, π-conjugated oligopeptides*

INTRODUCTION

Supramolecular self-assembly is a powerful bottom-up assembly strategy in nanotechnology that enables materials functionality to be controlled by noncovalent interactions between organic subunits.[1,2] Using this method, individual organic subunits can be designed to assemble into supramolecular structures via hydrogen bonding,[3] π−π stacking, metal−ligand coordination,[4] charge pairing,[5] hydrophobic forces, and/or steric repulsion.[6,7] It is noteworthy that these molecular-scale interactions govern self-assembly at the nanoscale, whereas higher-order complexity in structures can be derived from divergent kinetic pathways during the assembly process. In this way, hierarchical self-assembly of materials can be achieved through a combination of molecular-scale chemical forces and assembly kinetics.[8,9]

Peptides and amino acids are bioderived building blocks that can self-assemble into higher-order supramolecular structures via hydrogen bonding. From this view, peptides provide a high degree of structural control while offering additional advantages

Received: November 23, 2016
Accepted: January 9, 2017
Published: January 9, 2017

DOI: 10.1021/acsami.6b15068
ACS Appl. Mater. Interfaces 2017, 9, 3977−3984

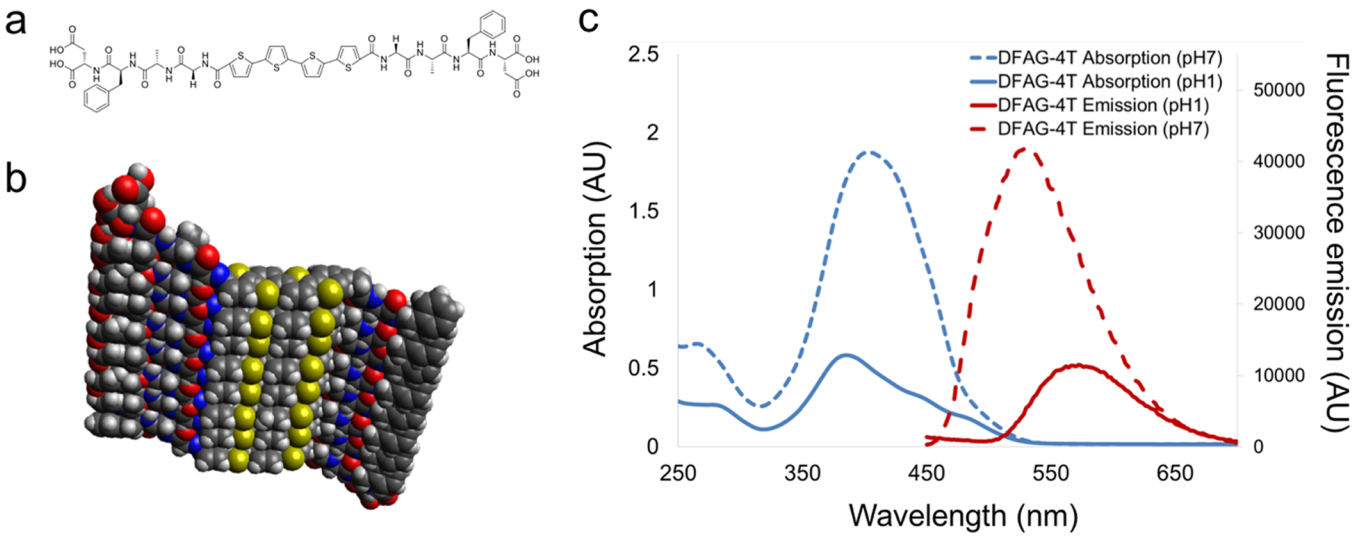

Figure 1. Structural and photophysical properties of unassembled and self-assembled π-conjugated oligopeptides. (a) Chemical structure of π-conjugated oligopeptides with quaterthiophene cores, denoted as DFAG-4T. (b) Schematic illustration of self-assembled structure of DFAG-4T. (c) Absorption (blue) and fluorescence (red) emission spectra of unassembled DFAG-4T under neutral pH conditions (dashed lines, pH 7) and assembled DFAG-4T under acidic conditions (solid lines, pH 1).

due to biocompatibility, versatility to chemical modification,[10] stability, and scalability,[11] all of which can be leveraged to generate complex structures.[12] Nanoscale self-assembly of peptides can be triggered by chemical cues such as solution acidity.[13] However, the pH-driven self-assembly of peptides into higher-order structures is highly sensitive to non-equilibrium effects such as assembly kinetics under certain conditions, yielding a diffusion-limited reaction front.[14] In some cases, it is known that direct addition of acid or acid vapor diffusion[15] into a peptide solution as an external triggering stimuli can induce rapid and localized protonation, thereby resulting in inhomogeneous peptide assembly due to the fast assembly rate of peptides in acidic conditions. To overcome this challenge, a few approaches have been developed to control assembly by changing solution pH in a controlled or homogeneous manner.[16,17] However, these approaches generally rely on controlling pH by addition of relatively large amounts of glucono-δ-lactone (GdL), which may affect self-assembled structures and further complicate the isolation and purification of assembled peptide from solution. To this end, there is a general need to further understand and control the kinetics of peptide self-assembly together with quantitative models to properly describe assembly.

One-dimensional π-conjugated molecules can serve as facile building blocks for soft electronic devices[18] due to their excellent processability[19] and control over electrical, optical, and optoelectronic properties.[20] For example, π-conjugated electroactive nanowires composed of aromatic units and hydrogen bonding motifs were shown to exhibit high mobility charge carriers on pulse radiolysis.[21] Compared to conventional synthetic π-conjugated polymers, biopolymer-synthetic polymer hybrid conjugates (e.g., polymer–peptide conjugates) exhibit exceptional structural and functional diversity as well as programmable control of noncovalent interactions via sequence control in biopolymer subunits.[22] In particular, synthetic oligopeptides with π-conjugated cores were shown to be ideal candidates for biobased electronic materials due to their unique biocompatible interfaces and water solubility.[23] However, the self-assembly of π-conjugated oligopeptides in solution is driven by pH or changes in ionic strength, which leads to difficulties and challenges in controlling the kinetics of nonequilibrium self-assembly at the microscale.

In this work, we study the nonequilibrium self-assembly of π-conjugated peptides using a combination of experiments and analytical modeling. By isolating an aqueous peptide solution within an immiscible organic layer, we effectively controlled the rate of diffusion of acid vapor used to trigger assembly, thereby enabling us to access both the reaction-dominated and diffusion-dominated regimes of assembly. Using this approach, we found that the morphology of self-assembled peptide fibers was affected by the kinetics of assembly, in particular observing that slower self-assembly rates generally lead to increasingly homogeneous fiber structures with higher degrees of anisotropy (i.e., needle-like structures). Moreover, we developed an analytical reaction–diffusion model to quantitatively describe the process of peptide assembly, and experimental results are directly compared to the model across a range of system parameters. Our results suggest that the diffusion of acid in the assembling peptide materials is much slower than that in pure water, likely due to an increase in local solution viscosity within the gel-like assembled peptide material and/or due to the dynamics of H^+ association/dissociation with amino acid residues on peptide backbones. In the limit of fast acid vapor diffusion in the organic layer relative to acid diffusion in the assembling peptide solution, acid tends to accumulate at the water/organic layer interface, thereby resulting in inhomogeneous self-assembly indicated by a ring-shaped assembly front that propagates from the outside to the inside of the peptide droplet. On the other hand, slower rates of acid vapor diffusion through the organic layer generally yield relatively homogeneous assembly reactions throughout the peptide solution. Taken together, these results can be used to understand and control the coupled reaction–diffusion process that guides the nonequilibrium self-assembly of synthetic oligopeptides.

EXPERIMENTAL METHODS

Materials. Sequence-defined synthetic oligopeptides with π-conjugated cores were synthesized using solid phase peptide synthesis (SPPS).[24,25] For these materials, a quaterthiophene (4T) core was

DOI: 10.1021/acsami.6b15068
ACS Appl. Mater. Interfaces 2017, 9, 3977–3984

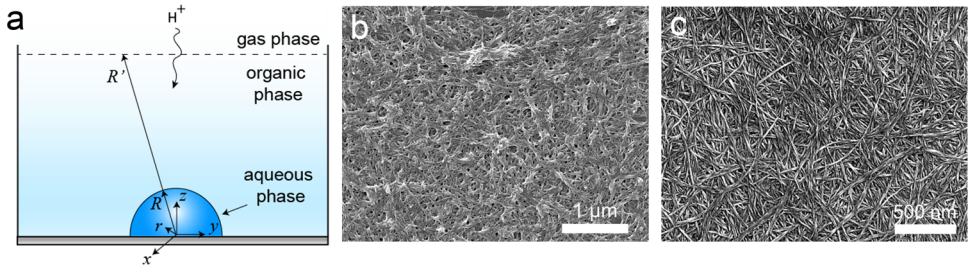

Figure 2. Tuning the assembly kinetics of π-conjugated oligopeptides. (a) Schematic illustration of the experimental setup using an organic isolation layer for acid vapor diffusion. (b and c) Scanning electron microscopy (SEM) images of self-assembled DFAG-4T fibers without and with organic layer (xylene) isolation, respectively.

flanked by symmetric oligopeptides with an amino acid sequence of Asp-Phe-Ala-Gly, yielding an overall sequence of HO-DFAG-4T-GAFD-OH (abbreviated as DFAG-4T) (Figure 1a). Materials were prepared according to previously reported procedures, and chemical characterization was found to match that of samples in prior work (Figures S2, S3, and S4).[26]

Self-Assembly via Organic Layer Isolation. A silicon (Si) wafer was cleaned with Piranha solution, rinsed with distilled/deionized (DI) water, and dried with nitrogen. A 60 μL aqueous solution droplet of DFAG-4T (at neutral pH) was added onto a clean Si wafer over an approximate area of 1.5 cm^2. An organic nonsolvent (toluene, xylene, hexane, cyclohexane, or silicone oil) was then carefully added on top of the droplet. To trigger assembly, the aqueous peptide droplet immersed within the organic isolation layer was moved into a sealed chamber, and a concentrated solution of acid (hydrochloric acid, HCl) was placed aside in the chamber. Following assembly, samples were prepared for structural and spectroscopic characterization by first removing the organic solvent. For volatile organic solvents (e.g., toluene, xylene, hexane, and cyclohexane), we first pumped out most of the organic solvent on top of the aqueous phase, followed by removal of the residual solvent by evaporation, which typically required several minutes. When using silicone oil as the organic layer, any residual traces of oil were carefully washed and removed using hexane. Following complete removal of the isolating organic layer, the assembled materials were carried forward for structural and spectroscopic characterization. For spectroscopic characterization of assembled peptides (e.g., absorption or fluorescence emission), we directly pipetted the peptide solution into microwell plates or cuvettes. For structural characterization, we allowed the aqueous phase to fully evaporate before analyzing samples, which typically required several hours for drying.

Structural and Optical Characterization. DFAG-4T samples were imaged using a Hitachi S4800 high-resolution Scanning Electron Microscope (SEM) at 5 kV. UV−Vis absorption spectra of unassembled and assembled DFAG-4T peptides were obtained using a Cary 5000 UV−Vis spectrometer (Agilent, USA), and fluorescence emission spectra were obtained using a TECAN infinite 200 PRO in 2 nm wavelength increments. The path length for absorption spectra is 10 mm, and the excitation wavelength for the fluorescence emission spectra is 370 nm.

Fluorescence Lifetime Imaging (FLIM). Fluorescence lifetime imaging microscopy (FLIM) was performed on unassembled and assembled DFAG-4T using a Zeiss LSM710 inverted microscope equipped with a Plan-Apochromat 20× objective (NA = 0.8). The FLIM system was first calibrated using a Rhodamine 6G standard (lifetime = 4.03 ns), where the edge of an aqueous drop of Rhodamine dye was illuminated in two-photon mode with a Ti:sapphire laser system (Mai-Tai, Spectra Physics), with light focused onto one of two high sensitivity nondescanned (GaAsP) detectors and directed to single-photon counting modules (ISS) for system calibration using ISS Vista software. Peptide samples were similarly prepared and mounted on the Zeiss LSM710 inverted microscope and first imaged using a QUASAR 34 channel spectral detector consisting of two standard PMTs and a 32 channel PMT array. After an area of interest was identified, scan area and speed were decreased to a 256 × 256 pixel array with a 6.3 μs pixel dwell time at 2× zoom, and the light path was redirected toward the single-photon counting modules. Data were analyzed for fluorescence lifetimes using the ISS Vista Vision software.

RESULTS AND DISCUSSION

We began by studying the self-assembly properties of DFAG-4T (Figure 1a). In general, DFAG-4T assembles into fiber-like structures in acidic conditions through noncovalent interactions. Under acidic conditions, the aspartic acid residue becomes protonated, thereby screening electrostatic repulsions and mediating the self-assembly of peptides into fibers via H-bonding between flanking peptides and $\pi-\pi$ stacking between adjacent quaterthiophene cores (Figure 1b). When the solution pH is decreased below ~5, the peak fluorescence emission wavelength of the assembled peptides is red-shifted from 520 to 560 nm (Figure 1c). In addition, fluorescence lifetime imaging microscopy (FLIM) generally shows that fluorescence lifetimes associated with the oligothiophene cores decrease for these peptides upon assembly (Figure S5), which can be attributed to an increase in the coherence length of π-conjugated subunits.[27]

Interestingly, we found that the morphology of self-assembled peptide fibers was highly dependent on the kinetics of self-assembly. A rapid transition to acidic conditions by abrupt exposure to concentrated acid vapor results in inhomogeneous assembled fiber morphologies and the formation of matted fibers. Although prior work has focused on the effect of the peptide primary amino acid sequence on the nanoscale assembled structures,[28] the effect of assembly kinetics on the morphology and microscopic structures is not fully understood. A common method for triggering peptide assembly is by direct addition of aqueous concentrated acid to a peptide solution or via concentrated acid vapor (HCl) diffusion into the aqueous peptide solution. In both cases, the delivery of acid and the reaction rate for assembly are both rapid relative to diffusional mixing inside the assembling peptide solution. Under these conditions, acid induces a rapid peptide assembly reaction initiating at the air/liquid interface, resulting in a diffusion-limited reaction front within the aqueous peptide solution. With this in mind, we hypothesized that the kinetics of peptide assembly can be controlled by tuning the rate of diffusion of acid vapor into the peptide solution. DFAG-4T is water-soluble but generally immiscible in common nonpolar organic solvents. Using this reasoning, we implemented a strategy to control the acid vapor diffusion process by isolating the peptide solution from the acid vapor atmosphere using an immiscible organic layer (Figure 2a). Here, we added an aqueous droplet containing unassembled peptide (at neutral pH) onto a solid substrate, followed by careful addition of the organic nonsolvent on top of the aqueous phase. In general,

DOI: 10.1021/acsami.6b15068
ACS Appl. Mater. Interfaces 2017, 9, 3977−3984

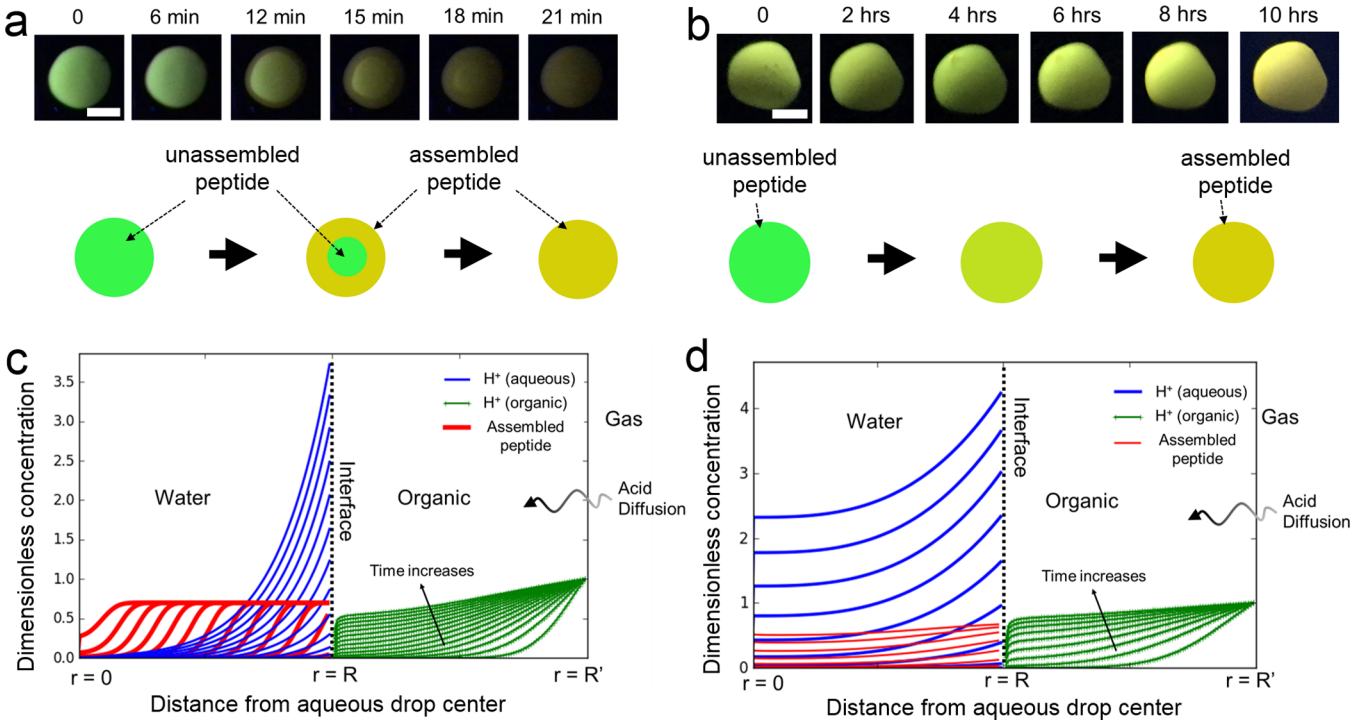

Figure 3. Reaction-controlled and diffusion-controlled assembly of π-conjugated oligopeptides using experiments and analytical modeling. (a) Optical micrographs of an aqueous DFAG-4T droplet undergoing assembly using toluene as the organic isolation layer. Under these conditions, reaction is rapid, and an assembly front is observed, as shown in the schematic. (b) Optical micrographs of an aqueous DFAG-4T droplet undergoing assembly using silicone oil as the organic isolation layer. Under these conditions, the assembly reaction is slowed, and no assembly front is observed, thereby yielding spatially homogeneous assembly as shown in the schematic. (c) Results from the coupled reaction−diffusion analytical model for reaction-dominated assembly (Type I, Da = 1000, α = 10). (d) Results from the coupled reaction−diffusion analytical model for diffusion-dominated assembly (Type II, Da = 0.1, α = 100). In both panels c and d, green lines show the acid concentration profile in the organic phase; blue lines show the acid concentration profile in the aqueous phase, and red lines show the concentration profile of the assembled peptide material. In these plots, acid diffuses from the saturated gas phase (right) through organic phase and into the aqueous peptide phase (left).

acid slowly diffuses through the organic layer, moves across the organic/aqueous interface, and eventually enters the aqueous peptide solution, which results in peptide assembly when the local pH value decreases below the pK_a of the peptide residues. The morphology of fibers assembled using the organic isolation method was determined using SEM, and these results show that increasingly homogeneous and discrete anisotropic fiber-like structures can be obtained by slowing the kinetics of assembly (Figures 2b and c). In addition, we used atomic force microscopy (AFM) to determine the average thickness of self-assembled peptide fibers (Figure S6). The average thickness was found to be approximately 6 nm, which is consistent with prior work suggesting that fibers form as single strands.[24]

Upon assembly, DFAG-4T peptides exhibit a pronounced red-shift in the peak fluorescence emission wavelength (from 520 to 560 nm) with a quenched emission intensity (Figure 1c). We used this spectral signature to monitor DFAG-4T self-assembly (1 mg/mL peptide, or ∼0.84 mM) by illuminating the samples using a visible light excitation source. We began by using the direct acid (HCl) vapor diffusion method to trigger self-assembly. When the HCl solution was placed near the DFAG-4T solution, the assembly reaction was rapid and completed within seconds under the direct vapor diffusion. On the other hand, the organic isolation method effectively extends the assembly reaction times from seconds to 20−30 min for toluene, xylene, or hexane (or >1 h for cyclohexane) due to the low solubility and slow transport rate of HCl through the liquid organic layer. Using the organic isolation method to mediate assembly using these solvents, we generally observed that peptide assembly proceeded via a reaction front indicated by a dark yellow ring around the periphery of aqueous peptide droplets and a bright green center consisting of unassembled DFAG-4T (Figure 3a). The spectral signature of the ring-like pattern shows that synthetic oligopeptides assemble from the outer regions of the droplet toward the inner region, which is consistent with a reaction-dominated assembly front.

Although the organic isolation method using low viscosity organic solvents (toluene, xylene, hexane, and cyclohexane) was found to extend the total time required for assembly from seconds to >1 h, this method nevertheless resulted in a spatially inhomogeneous assembly. For these organic liquids, peptides assemble under reaction-dominated conditions with an advancing peptide assembly front. Interestingly, we found that simply increasing the thickness of the organic layer did not lead to an increase in the total reaction time (Figure S7). To further control the kinetics of assembly, we used silicone oil (viscosity = 1000 cP at 25 °C) to greatly increase the assembly time, defined as the total time required for all of the DFAG-4T peptides to assemble. Using silicone oil as the isolation layer (thickness 1−10 cm), we found that the peptide solution assembled with a homogeneous pattern inside the droplet (over 10 h), generally showing a spatially uniform color change from light green to yellow in the absence of a ring pattern that is indicative of a reaction-controlled assembly front (Figure 3b). Moreover, the fluorescence emission spectrum of peptides

DOI: 10.1021/acsami.6b15068
ACS Appl. Mater. Interfaces 2017, 9, 3977−3984

assembled using silicone oil shows a red shift during assembly (Figure S8; fluorescence emission peak shifts from ~525 to ~550 nm after 10−12 h of assembly and further to ~575 nm after 24 h of assembly), which is consistent with the images shown in Figure 3b. Taken together, these results suggest that assembly occurs under diffusion-controlled conditions using silicone oil as the isolation layer.

To quantitatively describe the assembly process, we developed an analytical reaction−diffusion model for peptide assembly (Figures 3c and d). In general, three steps govern the assembly of synthetic oligopeptides under acidic conditions: first, HCl vapor diffuses through the organic layer and moves across the organic/aqueous interface; second, acid diffuses inside the aqueous peptide solution; finally, the aspartic acid residue on the flanking peptide sequence becomes predominately protonated at pH values lower than the pK_a (~4), thereby resulting in peptide assembly. We modeled the overall assembly process by considering reaction and/or diffusion in each of these three coupled steps. The full analytical model is described in the Supporting Information and Figure S1. In the following, we briefly describe the reaction−diffusion model and summarize the results. The aqueous droplet is assumed to have a hemispherical shape (Figure 2a), which justifies the use of spherical coordinates to solve the coupled reaction−diffusion problem. In the first step, the transport of acid through the organic layer is modeled by the diffusion equation:

$$\frac{\partial C_{H^+,o}}{\partial t} = D_{H^+,o}\nabla^2(C_{H^+,o}) \tag{1}$$

which can be written in spherical coordinates as

$$\frac{\partial C_{H^+,o}}{\partial t} = D_{H^+,o}\left(\frac{1}{r^2}\frac{\partial}{\partial r}\left(r^2\frac{\partial C_{H^+,o}}{\partial r}\right)\right) \tag{2}$$

where $C_{H^+,o}$ is the concentration of acid in the organic phase and $D_{H^+,o}$ is the diffusion coefficient of acid in the organic phase. In the second step, the species conservation equation for acid inside the aqueous peptide solution is given by a coupled reaction−diffusion equation:

$$\frac{\partial C_{H^+,aq}}{\partial t} = D_{H^+,aq}\left(\frac{1}{r^2}\frac{\partial}{\partial r}\left(r^2\frac{\partial C_{H^+,aq}}{\partial r}\right)\right) - k_f C_{H^+,aq} C_{P,i} \tag{3}$$

where $C_{H^+,aq}$ is the concentration of acid in the aqueous peptide solution, $D_{H^+,aq}$ is the diffusion coefficient of acid in the aqueous peptide solution, $C_{P,i}$ is the initial concentration of unassembled peptide, and k_f is the reaction rate constant for peptide assembly. Here, we assume that the assembly reaction can be modeled by a simple irreversible second order reaction: $H^+ + P \rightarrow PH^+$, where P is unassembled synthetic oligopeptide and PH^+ is assembled peptide. Equations 2 and 3 are partial differential equations for acid in the organic and aqueous phases, respectively, and each equation requires a separate initial condition and two boundary conditions. We proceed by rendering these equations dimensionless by characteristic concentration, length, and time scales for each phase. Using this approach, the dimensionless reaction−diffusion equation for acid in the aqueous phase is given by

$$\frac{\partial C_{H^+,aq}}{\partial t} = \frac{1}{r^2}\frac{\partial}{\partial r}\left(r^2\frac{\partial C_{H^+,aq}}{\partial r}\right) - Da C_{H^+,aq} \tag{4}$$

where the Damköhler number $Da = \frac{k_f C_{P,i} R^2}{D_{H^+,aq}}$ is a dimensionless group that gives the relative balance between the rate of the assembly reaction and the diffusion rate of acid in the aqueous solution. For simplicity, we assume that the diffusion coefficients of acid are equal in the assembled and unassembled regions of peptide inside the aqueous droplet, though we revisit this assumption in the discussion below. The boundary conditions at the organic/aqueous boundary effectively couple the partial differential equations given by eqs 2 and 3. In brief, the concentration of acid is assumed to rapidly reach an equilibrium distribution across the organic/aqueous phase given by a partition coefficient K, such that $C_{H^+,aq}(r = R,t) = KC_{H^+,o}$ $(r = R,t)$. In this way, the solubility of acid at the organic/aqueous phase is set by a fixed ratio, which is combined with a continuity of mass flux condition to ultimately determine the transport of acid across the interface. The boundary conditions at the organic/aqueous interface give rise to a second dimensionless group $\alpha = \frac{R'}{R}\frac{D_{H+,aq}}{D_{H+,o}}$, which physically describes the relative rate of diffusion of acid in the aqueous to the organic phase. Moreover, the model assumes that the forward rate constant for peptide assembly depends on the local acid concentration, which is related to the pK_a of the aspartic acid residue (Supporting Information). Finally, the assembled peptide species PH^+ is assumed to have a negligible diffusivity in solution such that $D_{H^+,aq} \gg D_{PH^+,aq}$

As observed in the experimental results shown in Figure 3, there are two types of self-assembly: inhomogeneous (Figure 3a) and homogeneous (Figure 3b) assembly within the aqueous peptide phase. These distinct types of assembly are determined by the relative rate of acid diffusion in aqueous to the organic phase (given by the dimensionless group α) and by the rate of the peptide assembly reaction relative to the rate of acid diffusion in the aqueous phase (given by the Damköhler number Da). When the diffusion rate of acid through the organic layer is relatively fast compared to the rate of diffusion in peptide solution, acid will accumulate at the organic/aqueous interface, thereby resulting in local and rapid peptide assembly. Consequently, the assembly front will propagate from the outside to the inside of the droplet, yielding ring-like pattern during the self-assembly process (referred to as Type I assembly, shown experimentally in Figure 3a with corresponding analytical results in Figure 3c). On the contrary, when the diffusion rate of acid through organic layer is relatively slow, the pH of the aqueous solution will decrease in a homogeneous fashion, thereby leading to spatially homogeneous self-assembly (referred to as Type II assembly, shown experimentally in Figure 3b with corresponding analytical results in Figure 3d). We can estimate the Damköhler number in our experiments as $Da \approx 10^5-10^6$, based on the system parameters of aqueous droplet radius R of 3 mm, diffusion coefficient of acid $D_{H^+,aq}$ of 3×10^{-9} m^2/s,[29] unassembled peptide concentration $C_{P,o}$ of 0.8 mM (corresponding to 1 mg/mL), and by assuming that the reaction rate constant for peptide assembly is equal to the forward rate constant for peptide protonation $k_f = 10^9$ M^{-1} s^{-1}.[30,31] However, the peptide assembly reaction is more complex than the simple second order protonation reaction assumed in the model and generally consists of multiple steps of assembly, which could reduce Da values by an order of magnitude. The dimensionless group α is estimated as $\alpha \approx 10^1$ for low viscosity organic solvents based on droplet radii R' of 10 cm and R of 3 mm and by assuming $D_{H,aq} \approx D_{H+,o}$ for low

DOI: 10.1021/acsami.6b15068
ACS Appl. Mater. Interfaces 2017, 9, 3977−3984

viscosity organic solvents such as toluene, hexane, and cyclohexane. Upon using silicone oil as the isolation layer, α increases by a factor of 1000 due to the large increase in solution viscosity for this solvent.

Using the coupled reaction−diffusion analytical model, we investigated the combined effects of Damköhler number *Da* and the relative ratio between the diffusion rates of acid in the aqueous to organic phase (given by α) on the dimensionless total reaction time (Figure 4). The total reaction time is defined as the time required for all peptides to assemble in solution, plotted in Figure 4 as the dimensionless total reaction time using the characteristic time scale for acid diffusion in water (Supporting Information). It should be noted that the characteristic diffusion time for acid in the water phase is $t_s = \frac{R^2}{D_{H+,aq}}$, which means the reaction time is proportional to the square of the droplet radius. Thus, larger droplets can result in a substantial increase in total reaction time. The results show that fast reaction rates (large *Da*) and relatively rapid diffusion in the organic layer (small α) lead to shorter reaction times. In general, these conditions give rise to a reaction-dominated assembly front, signifying inhomogeneous self-assembly, as shown in Figure 3c. On the other hand, relatively slow reaction rates (small *Da*) or slow acid diffusion through organic layer (large α) yields increasingly homogeneous concentration profiles of assembled peptide material. Interestingly, for small values of *Da* and α, ($Da \leq 1$ and $\alpha < 10$), the overall reaction time is fairly insensitive to acid diffusion rates. These results are consistent with experimental results showing that a simple increase in the volume of the organic layer does not change the total reaction time (Figure S7). Moreover, we also found that the total reaction time was fairly insensitive to changes in the critical pH value required for assembly (Figure S9). Finally, we can use the analytical model to broadly define parameter regimes under which the peptide assembly reaction is spatially inhomogeneous (Type I) or homogeneous (Type II), which are delineated in Figure 4.

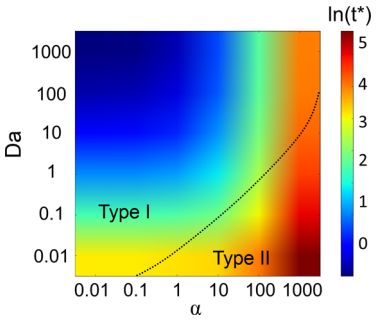

Figure 4. Phase plot of nonequilibrium peptide self-assembly as a function of the Damköhler number *Da* and the relative rate of acid diffusion in the aqueous to organic phases α. Here, t^* is the total dimensionless reaction time defined by the time required for all unassembled peptides to assemble in solution. The total reaction time is rendered dimensionless with the characteristic diffusion time for acid in the water as the time unit ($t^* = \frac{t_{assemble}}{t_{s,aq}}$). Type I and Type II refer to spatially inhomogeneous (reaction-controlled) and homogeneous (diffusion-controlled) self-assembly, respectively.

We further investigated the dynamics of assembly by tracking the position of the assembly front as a function of time for $Da \gg 1$ (Figure 5). Under these conditions, a ring-like pattern is observed in the aqueous peptide solution, suggestive of a reaction-controlled assembly front. Interestingly, experimental results show that the assembly front moves through the peptide solution nearly linearly in time (Figure 5a). Experimental data are compared to results from the analytical model (Figure 5b), and we generally find good agreement in terms of the overall dynamics from a qualitative perspective. In Figure 5b, note that analytical results are plotted as a function of dimensionless time, such that the characteristic time scale is related to the diffusion coefficient of acid in the assembling peptide solution. In reality, the diffusion of acid in the assembling peptide solution is a complicated function of association/disassociation events along the peptide backbone and the local solution viscosity, which is complicated by spatially inhomogeneous gelation within the aqueous peptide phase. In any event, experimental results show that the ring pattern visually emerges nearly halfway through the total reaction time, whereas the ring pattern emerges in analytical calculates around roughly one-third of the total reaction time. These results can be rationalized by considering that the analytical model assumes that the gas atmosphere above the organic layer is saturated with acid vapor at time zero, whereas in experiments, additional time is required for acid vapor to saturate the gas phase before diffusion through the organic layer.

CONCLUSIONS

In this work, we studied the nonequilibrium assembly of synthetic oligopeptides in aqueous solution using a combina-

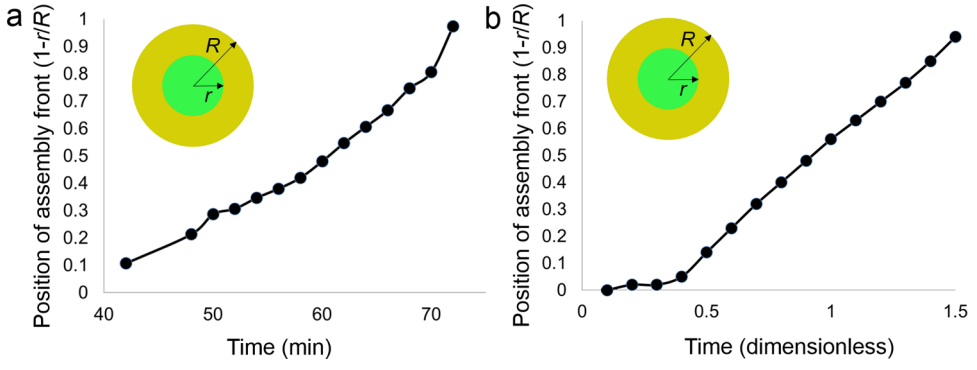

Figure 5. Dynamics of nonequilibrium peptide assembly studied using experiments and analytical modeling. (a) Experimental measurement of the position of the assembly front as a function of time using cyclohexane as the organic layer (thickness of 60 mm). (b) Results from the analytical model showing the position of the reaction assembly front with $Da = 1000$ and $\alpha = 10$.

DOI: 10.1021/acsami.6b15068
ACS Appl. Mater. Interfaces 2017, 9, 3977−3984

tion of experiments and analytical modeling. A coupled reaction−diffusion analytical model revealed the importance of two dimensionless groups controlling the peptide assembly process. In particular, the Damköhler number *Da* describes the rate of the peptide assembly reaction relative to that of acid diffusion inside the aqueous solution, whereas the dimensionless parameter α describes the relative rate of diffusion of acid in the aqueous and organic phases. The behavior of the peptide assembly process was studied across a wide range of *Da* and α, generally revealing reaction-dominated and diffusion-dominated regimes of assembly. In experiments, the delivery of acid to an aqueous peptide solution was controlled using an immiscible organic isolation layer, thereby allowing us to access both reaction-controlled and diffusion-controlled regimes of peptide assembly. Interestingly, our results show that the morphology of self-assembled synthetic oligopeptide fibers is affected by the assembly kinetics, such that rapid assembly generally leads to matted fibers, and relatively slower assembly results in homogeneous and anisotropic fiber morphologies. Using a viscous silicone oil as the organic isolation layer, peptide self-assembly was directed to occur under diffusion-controlled conditions, thereby yielding spatially homogeneous self-assembled peptide. Overall, this work provides a robust framework to understand the nonequilibrium self-assembly of π-conjugated oligopeptides, which provides new routes to kinetically tune nonequilibrium assembly of peptides and peptide derivatives for applications in organic electronics and bionanotechnology.

■ ASSOCIATED CONTENT

Supporting Information

The Supporting Information is available free of charge on the ACS Publications website at DOI: 10.1021/acsami.6b15068.

Analytical reaction−diffusion model for peptide assembly; analytical HPLC trace of DFAG-4T peptide; electrospray ionization mass spectrometry spectrum of purified DFAG-4T peptide; histograms showing distributions of fluorescence lifetimes for assembled and unassembled peptide; total reaction time of DFAG-4T self-assembly using different solvents for the organic isolation layer; fluorescence emission spectra for unassembled and assembled peptides using the organic isolation method with silicon oil as the isolation barrier; and effect of the critical assembly pH on the self-assembly of oligopeptides (PDF)

■ AUTHOR INFORMATION

Corresponding Author

*E-mail: cms@illinois.edu.

ORCID

Herdeline Ann M. Ardoña: 0000-0003-0640-1262

John D. Tovar: 0000-0002-9650-2210

Charles M. Schroeder: 0000-0001-6023-2274

Notes

The authors declare no competing financial interest.

■ ACKNOWLEDGMENTS

We thank Andrew Ferguson for useful discussions and the Frederick Seitz Materials Research Laboratory for facilities and instrumentation. This work was supported by the U.S. Department of Energy, Office of Science, Basic Energy Sciences (BES) under Award #SC-0011847. H.A.M.A. acknowledges a graduate fellowship through the Howard Hughes Medical Institute (International Student Research Fellowship) and the Schlumberger Foundation (Faculty for the Future Fellowship).

■ REFERENCES

(1) Aida, T.; Meijer, E. W.; Stupp, S. I. Functional Supramolecular Polymers. *Science* **2012**, *335*, 813.

(2) Burnworth, M.; Tang, L.; Kumpfer, J. R.; Duncan, A. J.; Beyer, F. L.; Fiore, G. L.; Rowan, S. J.; Weder, C. Optically Healable Supramolecular Polymers. *Nature* **2011**, *472*, 334−337.

(3) Desiraju, G. R. Supramolecular Synthons in Crystal Engineering—a New Organic Synthesis. *Angew. Chem., Int. Ed. Engl.* **1995**, *34*, 2311−2327.

(4) Brunsveld, L.; Folmer, B. J. B.; Meijer, E. W.; Sijbesma, R. P. Supramolecular Polymers. *Chem. Rev.* **2001**, *101*, 4071−4098.

(5) Tanrikulu, I. C.; Forticaux, A.; Jin, S.; Raines, R. T. Peptide Tessellation Yields Micrometre-Scale Collagen Triple Helices. *Nat. Chem.* **2016**, *8*, 1008.

(6) Hill, J. P.; Jin, W.; Kosaka, A.; Fukushima, T.; Ichihara, H.; Shimomura, T.; Ito, K.; Hashizume, T.; Ishii, N.; Aida, T. Self-Assembled Hexa-Peri-Hexabenzocoronene Graphitic Nanotube. *Science* **2004**, *304*, 1481−1483.

(7) Stupp, S. I.; Palmer, L. C. Supramolecular Chemistry and Self-Assembly in Organic Materials Design. *Chem. Mater.* **2014**, *26*, 507−518.

(8) Anderson, P. W. More Is Different. *Science* **1972**, *177*, 393−396.

(9) Xiao, S.; Tang, J.; Beetz, T.; Guo, X.; Tremblay, N.; Siegrist, T.; Zhu, Y.; Steigerwald, M.; Nuckolls, C. Transferring Self-Assembled, Nanoscale Cables into Electrical Devices. *J. Am. Chem. Soc.* **2006**, *128*, 10700−10701.

(10) Kol, N.; Adler-Abramovich, L.; Barlam, D.; Shneck, R. Z.; Gazit, E.; Rousso, I. Self-Assembled Peptide Nanotubes Are Uniquely Rigid Bioinspired Supramolecular Structures. *Nano Lett.* **2005**, *5*, 1343−1346.

(11) Gazit, E. Self-Assembled Peptide Nanostructures: The Design of Molecular Building Blocks and Their Technological Utilization. *Chem. Soc. Rev.* **2007**, *36*, 1263−1269.

(12) Whitesides, G.; Mathias, J.; Seto, C. Molecular Self-Assembly and Nanochemistry: A Chemical Strategy for the Synthesis of Nanostructures. *Science* **1991**, *254*, 1312−1319.

(13) Ardoña, H. A. M.; Tovar, J. D. Peptide Π-Electron Conjugates: Organic Electronics for Biology? *Bioconjugate Chem.* **2015**, *26*, 2290−2302.

(14) Mann, S. Self-Assembly and Transformation of Hybrid Nano-Objects and Nanostructures under Equilibrium and Non-Equilibrium Conditions. *Nat. Mater.* **2009**, *8*, 781−792.

(15) Hartgerink, J. D.; Beniash, E.; Stupp, S. I. Peptide-Amphiphile Nanofibers: A Versatile Scaffold for the Preparation of Self-Assembling Materials. *Proc. Natl. Acad. Sci. U. S. A.* **2002**, *99*, 5133−5138.

(16) Adams, D. J.; Butler, M. F.; Frith, W. J.; Kirkland, M.; Mullen, L.; Sanderson, P. A New Method for Maintaining Homogeneity During Liquid-Hydrogel Transitions Using Low Molecular Weight Hydrogelators. *Soft Matter* **2009**, *5*, 1856−1862.

(17) Morris, K. L.; Chen, L.; Raeburn, J.; Sellick, O. R.; Cotanda, P.; Paul, A.; Griffiths, P. C.; King, S. M.; O'Reilly, R. K.; Serpell, L. C.; Adams, D. J. Chemically Programmed Self-Sorting of Gelator Networks. *Nat. Commun.* **2013**, *4*, 1480.

(18) Schenning, A. P. H. J.; Meijer, E. W. Supramolecular Electronics; Nanowires from Self-Assembled [Small Pi]-Conjugated Systems. *Chem. Commun.* **2005**, 3245−3258.

(19) Kim, F. S.; Guo, X.; Watson, M. D.; Jenekhe, S. A. High-Mobility Ambipolar Transistors and High-Gain Inverters from a Donor−Acceptor Copolymer Semiconductor. *Adv. Mater.* **2010**, *22*, 478−482.

(20) Kim, F. S.; Ren, G.; Jenekhe, S. A. One-Dimensional Nanostructures of Π-Conjugated Molecular Systems: Assembly,

Properties, and Applications from Photovoltaics, Sensors, and Nanophotonics to Nanoelectronics. *Chem. Mater.* **2011**, *23*, 682−732.
(21) Schoonbeek, F. S.; van Esch, J. H.; Wegewijs, B.; Rep, D. B. A.; de Haas, M. P.; Klapwijk, T. M.; Kellogg, R. M.; Feringa, B. L. Efficient Intermolecular Charge Transport in Self-Assembled Fibers of Mono- and Bithiophene Bisurea Compounds. *Angew. Chem., Int. Ed.* **1999**, *38*, 1393−1397.
(22) Börner, H. G. Strategies Exploiting Functions and Self-Assembly Properties of Bioconjugates for Polymer and Materials Sciences. *Prog. Polym. Sci.* **2009**, *34*, 811−851.
(23) Besar, K.; Ardoña, H. A. M.; Tovar, J. D.; Katz, H. E. Demonstration of Hole Transport and Voltage Equilibration in Self-Assembled Π-Conjugated Peptide Nanostructures Using Field-Effect Transistor Architectures. *ACS Nano* **2015**, *9*, 12401−12409.
(24) Diegelmann, S. R.; Gorham, J. M.; Tovar, J. D. One-Dimensional Optoelectronic Nanostructures Derived from the Aqueous Self-Assembly of Π-Conjugated Oligopeptides. *J. Am. Chem. Soc.* **2008**, *130*, 13840−13841.
(25) Vadehra, G. S.; Wall, B. D.; Diegelmann, S. R.; Tovar, J. D. On-Resin Dimerization Incorporates a Diverse Array of [Small Pi]-Conjugated Functionality within Aqueous Self-Assembling Peptide Backbones. *Chem. Commun.* **2010**, *46*, 3947−3949.
(26) Sanders, A. M.; Dawidczyk, T. J.; Katz, H. E.; Tovar, J. D. Peptide-Based Supramolecular Semiconductor Nanomaterials Via Pd-Catalyzed Solid-Phase "Dimerizations. *ACS Macro Lett.* **2012**, *1*, 1326−1329.
(27) Spano, F. C.; Yamagata, H. Vibronic Coupling in J-Aggregates and Beyond: A Direct Means of Determining the Exciton Coherence Length from the Photoluminescence Spectrum. *J. Phys. Chem. B* **2011**, *115*, 5133−5143.
(28) Wall, B. D.; Zacca, A. E.; Sanders, A. M.; Wilson, W. L.; Ferguson, A. L.; Tovar, J. D. Supramolecular Polymorphism: Tunable Electronic Interactions within Π-Conjugated Peptide Nanostructures Dictated by Primary Amino Acid Sequence. *Langmuir* **2014**, *30*, 5946−5956.
(29) Lee, S. H.; Rasaiah, J. C. Proton Transfer and the Diffusion of H + and Oh− Ions Along Water Wires. *J. Chem. Phys.* **2013**, *139*, 124507.
(30) Bezrukov, S. M.; Kasianowicz, J. J. Current Noise Reveals Protonation Kinetics and Number of Ionizable Sites in an Open Protein Ion Channel. *Phys. Rev. Lett.* **1993**, *70*, 2352−2355.
(31) Yam, R.; Nachliel, E.; Gutman, M. Time-Resolved Proton-Protein Interaction. Methodology and Kinetic Analysis. *J. Am. Chem. Soc.* **1988**, *110*, 2636−2640.

DOI: 10.1021/acsami.6b15068
ACS Appl. Mater. Interfaces 2017, 9, 3977−3984